AIAA JOURNAL
Vol. 46, No. 9, September 2008

Topology Optimization Using Hyper Radial Basis Function Network

Aditya P. Apte* and Bo Ping Wang†
University of Texas at Arlington, Arlington, Texas 76019

DOI: 10.2514/1.28723

In this paper we present the application of a hyper radial basis function network as a topology description function. A hyper radial basis function network is used to parameterize the material distribution (density) for topology optimization. The density of each finite element in the continuum topology optimization domain is governed by a single network of hyper radial function bases. Thus, the topology optimization problem is to determine the parameters governing the hyper radial basis function network to satisfy certain design criteria. Here we present the solution to a minimum compliance topology design. A hyper radial basis function network is used to parameterize the material density during the finite element analysis stage. An efficient optimization algorithm that makes use of perturbation and sequential linear programming is developed to obtain the hyper radial basis function network parameters. Examples are presented to demonstrate the proposed approach and to compare it with the traditional solid isotropic microstructures with penalization topology optimization. Some of the advantages of the proposed approach are that it can yield checkerboard-free, manufacturable topologies using coarse-mesh finite element analysis models as opposed to the traditional approach, which requires fine meshes. This results in a reduction in the solution time for finite element analysis while conserving the ability to yield a smooth topology.

I. Introduction

TOPOLOGY optimization [1] aims at obtaining the "best" possible arrangement of the given volume of structural material within a spatial domain to obtain an optimal mechanical performance of the concept design. The topology optimization is a material distribution problem in which the material content of each of the points of the reference domain must be determined. The traditional approach to solving this problem is to mesh the reference domain and obtain the material content of each element to determine the optimal material distribution. If the material content of an element is above the cutoff level (corresponding to the percentage of total material), a material density of 1 is assigned to that element, whereas if the material content of an element is below the cutoff level, a void (or a material density of 0) is assigned to that element. Also, various methods have been suggested by researchers to model the intermediate densities (e.g., the level set method [2]) to improve the performance of this traditional approach. All these methods compute the optimal density of each element; hence, there must be as many design variables as the number of finite elements. The number of elements must be sufficient to obtain a correct representation of geometrical features as well as a correct physical response.

The idea of using a topology description function (TDF) stems from the fact that the number of elements required in a finite element analysis (FEA) model to represent the geometrical features far exceeds that required to obtain a correct physical response. As such, describing the geometrical features using a TDF instead of the traditional approach would lead to a drastic reduction in the number of parameters required to describe the geometrical features, assuming that a TDF can be represented by a small number of parameters as compared with the corresponding number of elements required. This would permit the use of a coarse mesh (sufficient to obtain a correct physical response) in solving the FEA problem. Modeling material densities as TDFs also helps get rid of checkerboard patterns as observed by Stolpe and Svanberg [3]. They used finite element approximation for continuous material distribution in a fixed design space. The research on the use of TDFs has started gaining popularity recently. De Ruiter and van Keulen [4] used a network of Gaussian basis functions to define the topology description function while using the solid isotropic microstructures with penalization (SIMP) method [5]. The location and widths of these bases were fixed and the only variables were the basis weights. They used as many bases as the number of finite elements. Thus, the number of design variables remained same as those used in the SIMP method. Wang et al. [6] used the radial basis function multiquadric splines to construct the implicit level set function with a high level of accuracy and smoothness and to discretize the original initial value problem into an interpolation problem. Again, the location and width of their bases were fixed. A wavelet is an another way to represent the density function in terms of basis functions that are linked to length scales and are not directly coupled to the finite element mesh of the analysis [7]. Cui et al. [8] used Bezier curves for a morphological representation of structural geometry. All the approaches outlined herein are not very user friendly in terms of understanding the effect of the change in the design variable on the material distribution. The hyper radial basis function network (HRBFN) is intuitive and can be made user interactive. The user can interactively change the location, width, orientation, or weight of one or more bases and see the effect on the structural topology. This approach is under investigation and we plan to report the results in a future paper. In this work, the application of a HRBFN as a TDF is presented.

The layout of the rest of the paper is as follows. HRBFN is briefly described in Sec. II. In Sec. III, HRBFN is coupled with an FE analysis to obtain structural compliance (strain energy). A semi-analytical sensitivity (to the HRBFN parameters) analysis for compliance is briefly outlined. Section IV describes the algorithm to solve the topology optimization problem using sequential linear programming. Numerical examples are presented in Sec. V, followed by conclusions.

II. Hyper Radial Basis Function Network

The parametric model for a hyper radial basis network [9,10] can be represented as

Presented as Paper 1814 at the 47th AIAA/ASME/ASCE/AHS/ASC Structures, Structural Dynamics, and Materials Conference, Newport, RI, 1–4 May 2006; received 5 November 2006; revision received 5 January 2008; accepted for publication 29 March 2008.

*Graduate Student, Department of Mechanical Engineering; also Bioinformaticist, Washington University School of Medicine, Saint Louis, Missouri. Student Member AIAA.

†Professor, Department of Mechanical Engineering. Senior Member AIAA.

$$f(X) = \sum_{i=1}^{r} w_i \phi_i(\|X - \mu_i\|, \alpha_i, \theta_i) \tag{1}$$

where r is the number of bases, $X \in R^n$ is an input vector, ϕ_i is the basis function, w_i are the weights of the network, $\mu_i = (\mu_{i1}, \mu_{i2} \cdots \mu_{in})$ is the center vector of the ith basis, $\alpha_i = (\alpha_{i1}, \alpha_{i2} \cdots \alpha_{ip})$ is the angle vector of the ith node where p is the number of parameters required to define the orientation of the basis in an n-dimensional space, $\theta_i = (\theta_{i1}, \theta_{i2} \cdots \theta_{in})$ is the bandwidth vector of the ith node, and $\| \ \|$ denotes the Euclidean norm. The hidden layer for this network represents the approximation parameters w_i, μ_i, α_i, and θ_i to characterize the material distribution. The output layer represents the material distribution as a continuous function of the hidden parameters. In this paper, we restrict ourselves to a 2-D design space and, hence, $X \in R^2$, that is, $n = 2$ and $p = 1$. The basis function of the network is chosen to be a Gaussian function, which can be represented as

$$\phi_i(\|X - \mu_i\|, \alpha_i, \theta_i) = e^{-g^2} \tag{2}$$

where

$$g^2 = \Delta x^T [T^T] \begin{bmatrix} \frac{1}{\theta_{i1}} & 0 \\ 0 & \frac{1}{\theta_{i2}} \end{bmatrix} [T] \Delta x$$

is always positive and

$$T = \begin{bmatrix} \cos(\alpha_{i1}) & \sin(\alpha_{i1}) \\ -\sin(\alpha_{i1}) & \cos(\alpha_{i1}) \end{bmatrix}, \quad \Delta x = \begin{Bmatrix} \bar{\mu}_1 - \mu_{i1} \\ \bar{\mu}_2 - \mu_{i2} \end{Bmatrix}, \quad X = (\bar{\mu}_1, \bar{\mu}_2)$$

Thus, the material distribution can be approximated as shown in Eq. (3):

$$\rho(X) = \rho(X, w, \mu, \alpha, \theta) = \sum_{i=1}^{r} w_i e^{-g_i^2} \tag{3}$$

where w refers to network weights for material distribution (i.e., the basis weights w_i, $i = 1$ to r), $\mu = (\mu_1, \mu_2 \cdots \mu_r)$ refers to the center locations for the r bases, $\alpha = (\alpha_1, \alpha_2 \cdots \alpha_r)$ refers to the angle parameters for the r bases, and $\theta = (\theta_1, \theta_2 \cdots \theta_r)$ refers to the bandwidth parameter for the r bases. Note that $6r$ parameters are required to describe the material distribution or TDF and, hence, to train the network for two-dimension problems. As an example, consider a 2-D basis with a center location of (1.5, 1), a bandwidth of (0.5, 1) and an angle of (30 deg). Figure 1 shows the magnitude and shape of this basis in a 2-D space. Figure 2 shows the contour of the basis at a magnitude of 0.05.

Now, consider a 2-D hyper radial basis network with 2 bases. For the first basis, let the weight, center location, bandwidth, and angle be (1), (1.5, 1), (0.3, 0.1), and (30 deg), respectively. For the second basis, let the weight, center location, bandwidth, and angle be (1), (2, 2), (0.25 0.05) and (120 deg), respectively. Figure 3 shows the magnitude and shape of this network in a 2-D space. Figure 4 shows the contour of the basis at a magnitude of 0.05.

The examples presented in this section demonstrate the flexibility of the HRBFN in terms of magnitude and orientation to model the material distribution in a topology optimization. Section III describes the coupling of the HRBFN and the FEA.

III. Implementation of the Hyper Radial Basis Function Network into a Finite Element Analysis

As stated before, the physical response of system (or structure) is calculated by a finite element analysis with the material density distribution governed by the HRBFN. In this paper we are interested in minimum compliance design; hence, the physical response is the compliance (strain energy) of the system. For a linear static FE model, the equation relating nodal degrees of freedom and the nodal loads is

$$KU = P \tag{4}$$

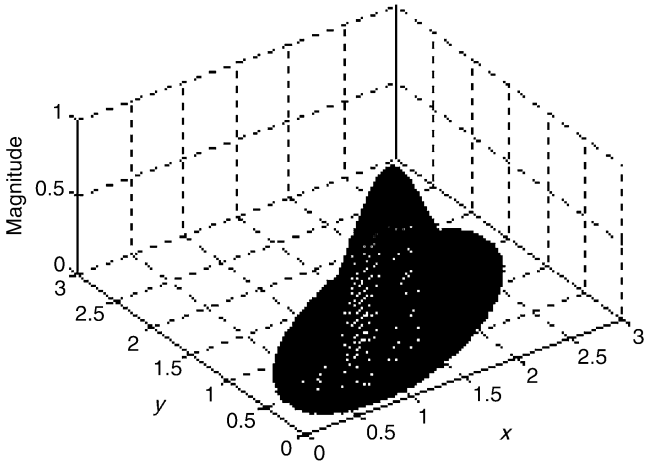

Fig. 1 Shape and magnitude of the 2-D hyper radial basis.

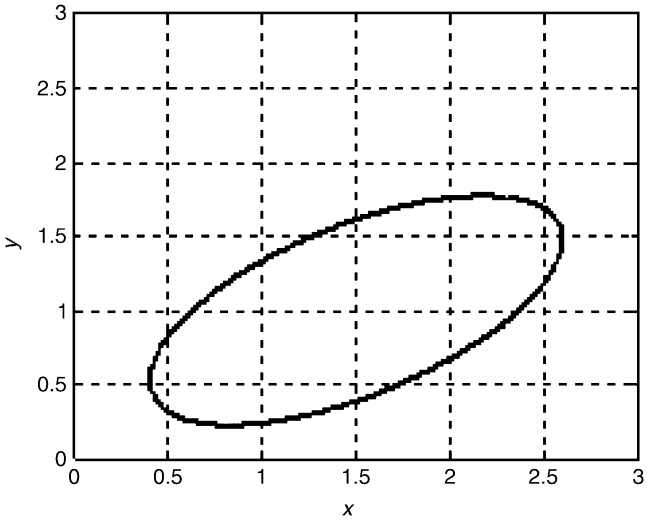

Fig. 2 Shape of the 2-D hyper radial basis.

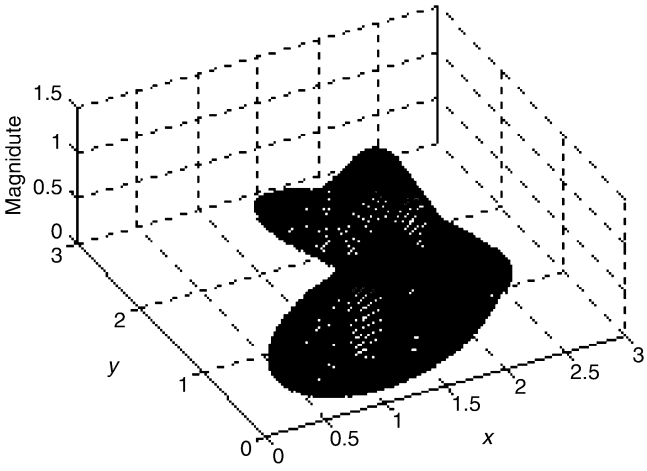

Fig. 3 Shape and magnitude of the 2-D hyper radial basis network.

where U is the vector of global nodal degrees of freedom, P is the vector of global nodal loads, and K is the global stiffness matrix assembled from the elemental stiffness matrices:

$$K = \sum_{j=1}^{N_e} (\rho_j^{n^*} + \rho_{\text{reg}})(K_e)_j \tag{5}$$

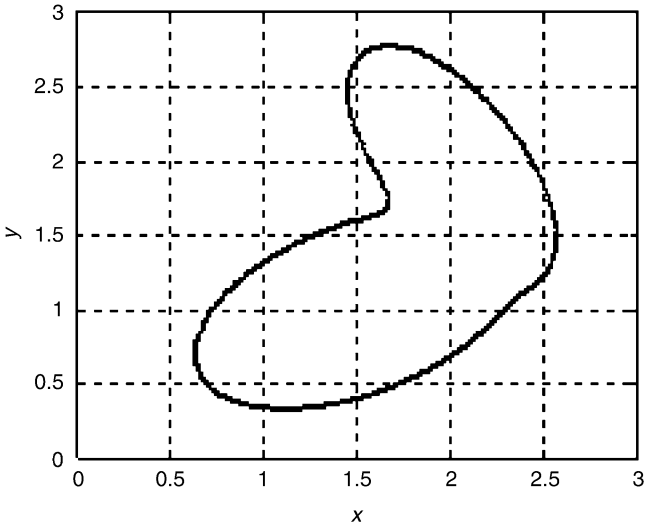

Fig. 4 Shape of the 2-D hyper radial basis network.

where $(K_e)_j$ is the elemental stiffness matrix for the jth element and ρ_{reg} is the regularization term to avoid singularity in the stiffness matrix. $\rho_{\text{reg}} = 10^{-4}$ was used for the examples presented in Sec. V.

The density of element j is governed by the HRBFN and can be written as shown in Eq. (6):

$$\rho_j = \rho_j(Xe_j, Ye_j) = \sum_{i=1}^{r} w_i e^{-g_i^2} \tag{6}$$

where

$$g^2 = \Delta x^T [T^T] \begin{bmatrix} \frac{1}{\theta_{i1}} & 0 \\ 0 & \frac{1}{\theta_{i2}} \end{bmatrix} [T] \Delta x, \qquad T = \begin{bmatrix} \cos(\alpha_{i1}) & \sin(\alpha_{i1}) \\ -\sin(\alpha_{i1}) & \cos(\alpha_{i1}) \end{bmatrix}$$

as before, and

$$\Delta x = \begin{Bmatrix} \bar{\mu}_1 - \mu_{i1} \\ \bar{\mu}_2 - \mu_{i2} \end{Bmatrix}, \qquad X = (\bar{\mu}_1, \bar{\mu}_2) = (Xe_j, Ye_j)$$

where N_e is the number of elements for the finite element analysis and n^* is the power of density. $n^* = 3$ was used for the examples presented. Note that the results deteriorated when $n^* > 3$ was used, whereas the convergence was found to be slow for $n^* = 1$. This behavior is similar to that already researched for traditional density method algorithms. This paper does not address the optimal value of n^* in particular.

Note that the density across each element is assumed to be constant and evaluated at its centroidal coordinates (Xe_j, Ye_j). The procedure illustrated was implemented in MATLAB®[‡] making use of matrix algebra. The compliance (or strain energy) of the system is given by

$$C = \tfrac{1}{2} U^T K U \tag{7}$$

A sensitivity analysis is required for the efficient convergence of an optimizer. From Eqs. (4) and (7),

$$\frac{\mathrm{d}C}{\mathrm{d}\hbar} = \frac{\mathrm{d}(U^T K U)}{2\mathrm{d}\hbar} = \frac{\mathrm{d}(U^T P)}{2\mathrm{d}\hbar} = \frac{\mathrm{d}U^T}{2\mathrm{d}\hbar} P \tag{8}$$

where $\hbar$ is a design variable. Specifically, $\hbar = (w, \mu, \alpha \text{ or } \theta)$ for each basis, or

$$\frac{\mathrm{d}C}{\mathrm{d}\hbar} = -\frac{1}{2} U^T \frac{\mathrm{d}K}{\mathrm{d}\hbar} U \tag{9}$$

$\frac{\mathrm{d}K}{\mathrm{d}\hbar}$ in Eq. (9) can be computed analytically or by using an approximate method such as a finite difference or complex variable method [11]. Because the examples presented in this paper involve a small number of degrees of freedom (2 DOF) and bases (design variables), an approximate sensitivity analysis method is not computationally prohibitive. An analytical sensitivity computation will no doubt speed up the optimization process and is preferred for large-scale problems involving computationally expensive stiffness matrices. A complex variable method is computationally stable and more accurate compared with the finite differencing and was used for the sensitivity analysis in the examples presented.

[‡]Data available online at http://www.mathworks.com [retrieved 1 June 2008].

IV. Optimization Algorithm

Because the material distribution is governed by the HRBF, a nonlinear function of locations, bandwidths, angles, and intensities for the bases, the optimization problem is challenging. We linearize this problem using Taylor's series and solve it using sequential linear programming (SLP). To ensure the proper convergence of SLP, the starting design must be close to the optimal. We divide our optimization process into the following two parts: 1) a perturbation algorithm to obtain a minimum compliance design close to the optimal solution, and 2) sequential linear programming starting from the design yielded by part 1 to obtain the optimal solution.

A. Perturbation Algorithm to Obtain the Starting Point for Sequential Linear Programming

Figure 5 briefly describes the perturbation algorithm. Here we perturb the nonlinear design variables' location and angle based on the signs of their sensitivities. The nonlinear design variable bandwidth is perturbed based on the sign of the difference between its sensitivity and the median of sensitivities of the bandwidths of all the bases. This is because the sensitivity of compliance with respect to the bandwidth is always negative for structures with symmetric (positive definite) stiffness matrices. This is explained in more detail by Eqs. (10) and (14).

Consider the first bandwidth for the ith base. Equation (9) can be rewritten for the bandwidth variable as Eq. (10):

$$\frac{\mathrm{d}C}{\mathrm{d}\theta_{i1}} = -\frac{1}{2} U^T \frac{\mathrm{d}K}{\mathrm{d}\theta_{i1}} U \tag{10}$$

Substituting Eq. (6) in Eq. (10), we obtain Eq. (11):

$$\frac{\mathrm{d}C}{\mathrm{d}\theta_{i1}} = -\frac{1}{2} U^T \frac{\mathrm{d}\sum_{j=1}^{N_e} (\rho_j^{n^*} + \rho_{\text{reg}})(K_e)_j}{\mathrm{d}\theta_{i1}} U \tag{11}$$

Substituting the density from Eq. (3) in Eq. (11), we obtain Eq. (12):

$$\frac{\mathrm{d}C}{\mathrm{d}\theta_{i1}} = -\frac{1}{2} U^T \frac{\mathrm{d}\sum_{j=1}^{N_e} ((\sum_{i=1}^{r} w_i e^{-g_i^2})^{n^*} + \rho_{\text{reg}})(K_e)_j}{\mathrm{d}\theta_{i1}} U \tag{12}$$

Differentiating Eq. (11) with respect to the bandwidth, we obtain the sensitivity as shown in Eq. (13):

$$\frac{\mathrm{d}C}{\mathrm{d}\theta_{i1}} = -\frac{1}{2} U^T \left[\sum_{j=1}^{N_e} \frac{n^* (Xe_j - \mu_{i1})^2 \rho_j^{n^*} (K_e)_j}{\theta_{i1}^2} \right] U \tag{13}$$

Similarly, for the second bandwidth of the ith base, we obtain the sensitivity as shown in Eq. (14):

$$\frac{\mathrm{d}C}{\mathrm{d}\theta_{i2}} = -\frac{1}{2} U^T \left[\sum_{j=1}^{N_e} \frac{n^* (Ye_j - \mu_{i2})^2 \rho_j^{n^*} (K_e)_j}{\theta_{i2}^2} \right] U \tag{14}$$

Note that, in Eqs. (13) and (14), the term in [] is always positive definite. Hence, the sensitivity given by Eqs. (13) and (14) is always negative. The linear variable weight is computed using linear programming by imposing the constraints as shown in Fig. 5.

B. Sequential Linear Programming Starting from the Solution of the Perturbation Algorithm

The optimization problem can be stated as shown in Eqs. (7), (15), and (16). Minimize $C = \frac{1}{2} U^T K U$ subject to

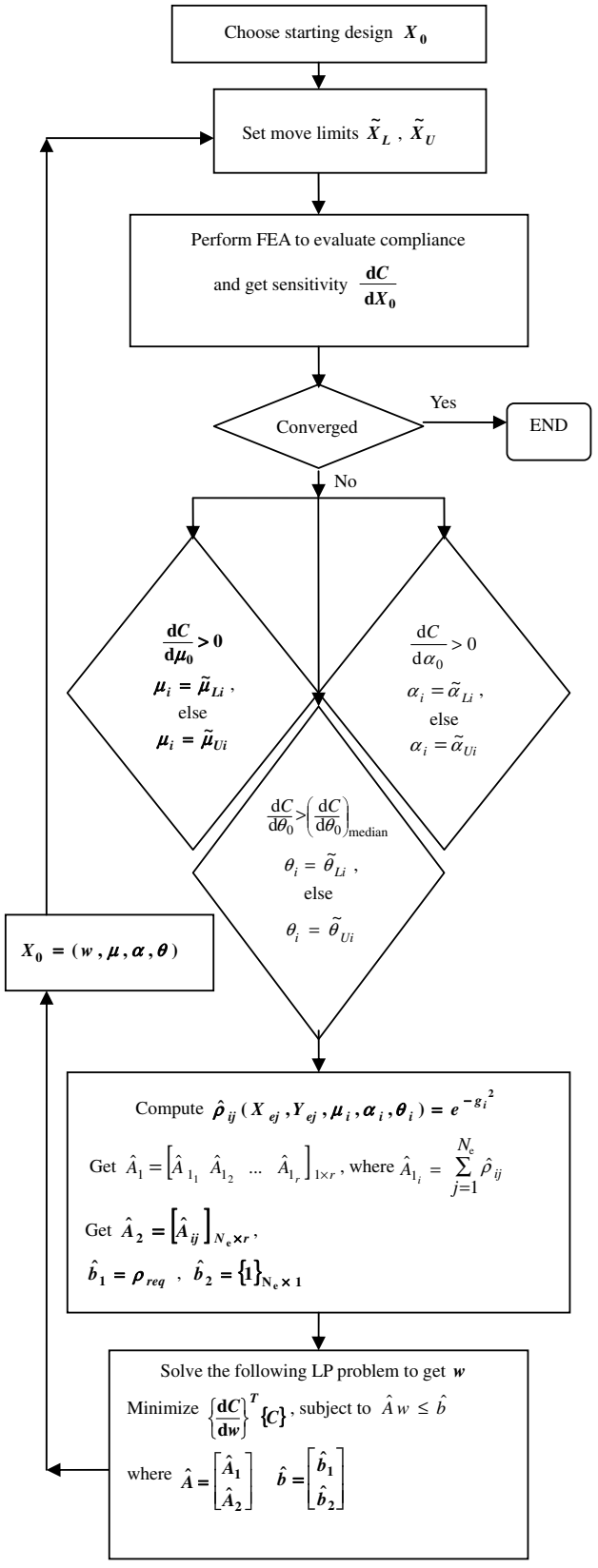

Fig. 5 Perturbation algorithm.

$$\sum_{j=1}^{N_e} \rho_j \le \rho_{\text{req}} \tag{15}$$

and

$$\rho_j \le 1 \quad \text{for} \quad j = 1 \text{ to } N_e \tag{16}$$

where ρ_{req} is the total volume of material to be retained and N_e is the number of elements in the FEA model.

The standard form of the LP problem is as follows: calculate x to minimize $f^T x$ subject to $Ax \le B$.

Hence, the objective and constraints in our compliance minimization problem should be formulated to be compatible with the LP formulation. The objective function can be reformulated using Taylor's series expansion for compliance up to the first order as follows:

$$C = C_{0j} + \sum_{i=1}^{N_{\text{dv}}} \frac{\partial C}{\partial x_i}(x_i - x_{i0}) \tag{17}$$

$$C = C_{0j} - \sum_{i=1}^{N_{\text{dv}}} \frac{\partial C}{\partial x_i} x_{i0} + \sum_{i=1}^{N_{\text{dv}}} \frac{\partial C}{\partial x_i} x_i \tag{18}$$

where N_{dv} is the number of design variables. Specifically, $N_{\text{dv}} = 6r$ as stated earlier.

Note that the first two terms in Eq. (18) are constant and independent of the new design. Hence, minimizing C in Eq. (18) is same as minimizing Eq. (19):

$$C = \sum_{i=1}^{N_{\text{dv}}} \frac{\partial C}{\partial x_i} x_i \tag{19}$$

In matrix form,

$$C = [F]^T \{x\} \tag{20}$$

where $[F] = \frac{\partial C}{\partial x}$ is the gradient of compliance evaluated at current design x_0 and has the dimension $N_{\text{dv}} \times 1$, and x is a vector of the design variables, that is, the HRBFN parameters, and has the dimension $N_{\text{dv}} \times 1$.

The constraint Eq. (15) can be formulated as follows:

$$\sum_{j=1}^{N_e} \rho_j \le \rho_{\text{req}}$$

Using Taylor's series expansion and retaining only the first order term,

$$\sum_{j=1}^{N_e} \left(\rho_{0j} + \sum_{i=1}^{N_{\text{dv}}} \frac{\partial \rho_j}{\partial x_i}(x_i - x_{i0}) \right) \le \rho_{\text{req}} \tag{21}$$

$$\sum_{j=1}^{N_e} \sum_{i=1}^{N_{\text{dv}}} \frac{\partial \rho_j}{\partial x_i} x_i \le \rho_{\text{req}} - \sum_{i=1}^{N_e} \rho_{0j} + \sum_{j=1}^{N_e} \sum_{i=1}^{N_{\text{dv}}} \frac{\partial \rho_j}{\partial x_i} x_{i0} \tag{22}$$

In matrix form,

$$A_1 x \le b_1 \tag{23}$$

where

$$A_1 = \sum_{j=1}^{N_e} \frac{\partial \rho_j}{\partial x}$$

is of the dimension $1 \times N_{\text{dv}}$, x is a vector of the design variables, that is, the HRBFN parameters, and has the dimension $N_{\text{dv}} \times 1$, and

$$b_1 = \rho_{\text{req}} - \sum_{j=1}^{N_e} \rho_{0j} + \sum_{j=1}^{N_e} \sum_{i=1}^{N_{\text{dv}}} \frac{\partial \rho_j}{\partial x_i} x_{i0}$$

is of the dimension 1×1.

The constraint Eq. (16) can be formulated as follows:

$$\rho_j \le 1$$

Using Taylor's series expansion and retaining only the first order term,

$$\rho_{0j} + \sum_{i=1}^{N_{\text{dv}}} \frac{\partial \rho_j}{\partial x_i}(x_i - x_{i0}) \leq 1 \quad \text{for} \quad j = 1 \text{ to } N_e \tag{24}$$

$$\sum_{i=1}^{N_{\text{dv}}} \frac{\partial \rho_j}{\partial x_i} x_i \leq 1 - \rho_{0j} + \sum_{i=1}^{N_{\text{dv}}} \frac{\partial \rho_j}{\partial x_i} x_{i0} \tag{25}$$

In matrix form,

$$A_2 x \leq b_2 \tag{26}$$

where $A_2 = \frac{\partial \rho}{\partial x}$ is of the dimension $N_e \times N_{\text{dv}}$, x is a vector of the design variables, that is, the HRBFN parameters, and has the dimension $N_{\text{dv}} \times 1$, and

$$b_2 = \{1\}_{N_e \times 1} - \rho_{0j} + \sum_{i=1}^{N_{\text{dv}}} \frac{\partial \rho_j}{\partial x_i} x_{i0}$$

is of the dimension $N_e \times 1$.

The constraint Eqs. (15) and (16) can together be put into matrix form by combining Eqs. (23) and (26) as

$$\begin{bmatrix} A_1 \\ A_2 \end{bmatrix} \{x\} \leq \begin{Bmatrix} b_1 \\ b_2 \end{Bmatrix} \tag{27}$$

Equations (20) and (27) represent the standard form for the LP problem. This SLP problem can be solved using the commercial optimization toolbox available within MATLAB® and MOSEK,[§] to name a few.

V. Numerical Examples

Three examples are presented to demonstrate the advantages of using the HRBFN as a TDF. Figure 6 (example 1) shows a cantilever beam fixed at left edge and horizontal axial loading at the midpoint of right edge. The objective is to get a minimum compliance design using 40% of the total material. The first example uses a coarse finite element analysis grid (8×4). Figure 7 shows the optimal topology obtained by a traditional method (Sigmund [12]) using a filtering scheme so that the top 40% of densities are retained. Figure 8 shows the optimal location of the HRBFN bases. Figure 9 shows the topology obtained by the proposed approach using 10 bases, the same mesh size as that of the traditional method, and the same filtering scheme. Figure 10 shows the unfiltered plot for the traditional method. Figure 11 shows the result of the perturbation algorithm, which serves as a starting point for sequential linear programming.

It is evident that the filtered plot for the traditional method does not provide a good idea about what the topology should look like. As opposed to that, the proposed approach provides a correct representation of the topology, and the topology is quite close to being "manufacturable." Note that the unfiltered plot for the traditional topology shown in Fig. 10 gives some idea about what the final topology should look like, but it is nowhere close to being manufacturable. In more complicated structures, the unfiltered plots might be difficult to interpret and may lead to incorrect designs. The number of finite element analyses used for both the approaches was fixed to be 40. The value of compliance for the HRBFN approach was 1.4941×10^{-6}, whereas the value of compliance for the traditional approach was found to be 2.8384×10^{-6}. Note that the value of compliance in the case of the traditional method might change significantly because the topology needs to be modified for manufacturing. But, in the case of the HRBFN approach, the value of compliance would remain more or less the same because the topology obtained is close to being manufacturable.

The selection of the lower and upper bounds for the HRBFN parameters is quite general and can be automated. The weight parameter always lies between 0 and 1. The location parameter is

[§]Data available online at http://www.mosek.com [retrieved 1 June 2008].

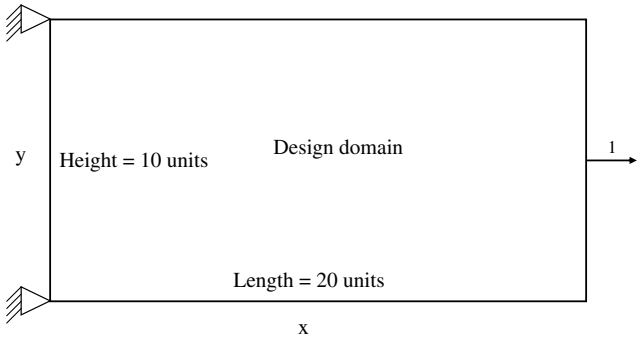

Fig. 6 Boundary conditions and loading for example 1, which uses an 8 × 4 FEA mesh.

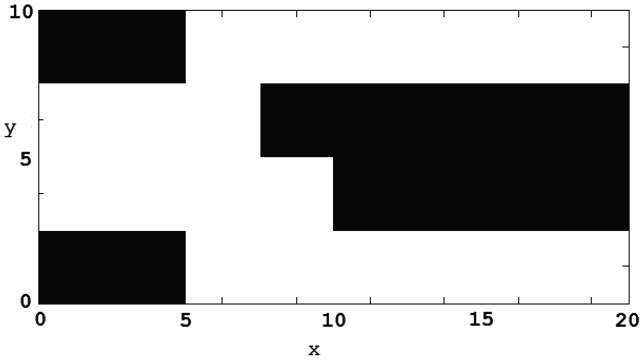

Fig. 7 Result of traditional SIMP topology optimization for example 1, filtered.

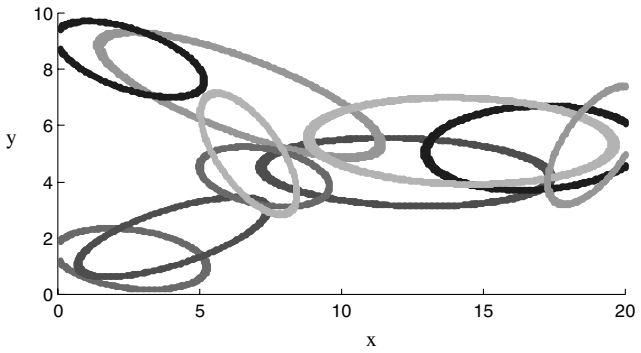

Fig. 8 Optimized locations and shapes of HRBFN bases for example 1.

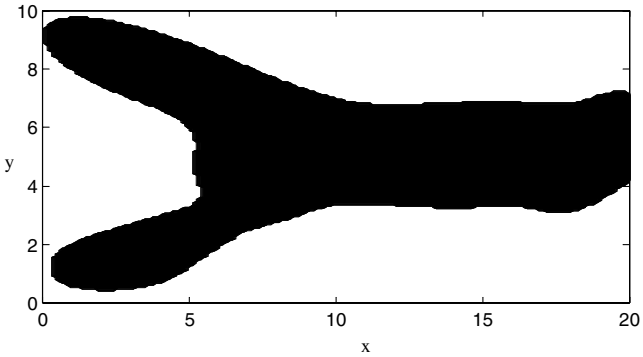

Fig. 9 Result of HRBFN-based topology optimization for example 1.

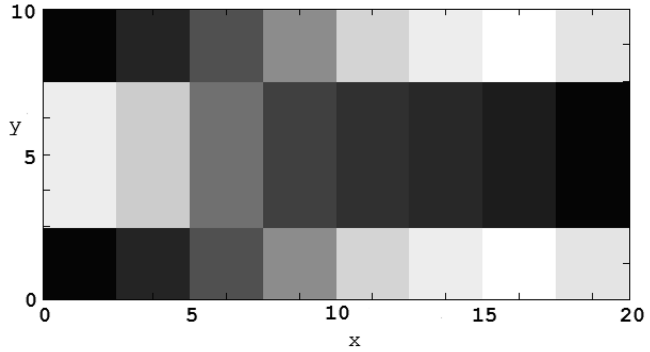

Fig. 10 Result of traditional SIMP topology optimization for example 1, unfiltered.

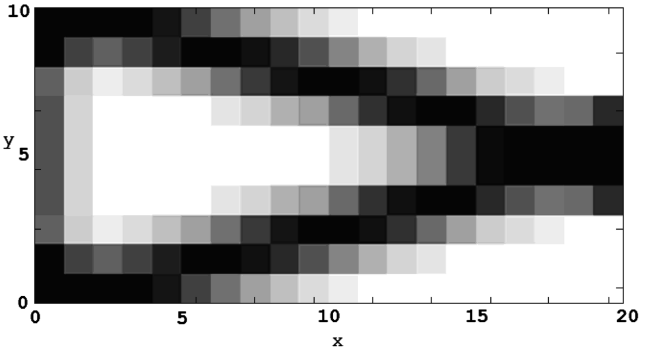

Fig. 13 Result of traditional SIMP topology optimization for example 2, unfiltered.

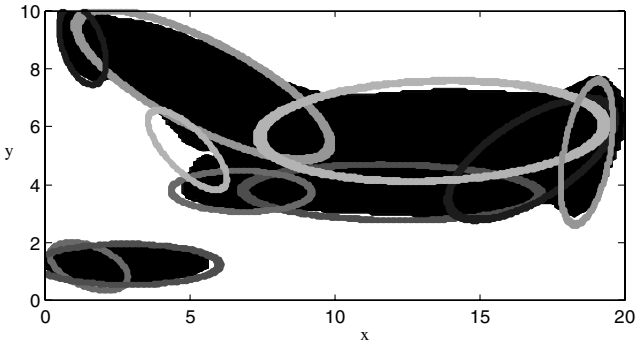

Fig. 11 Result of perturbation algorithm for HRBFN-based topology optimization for example 1.

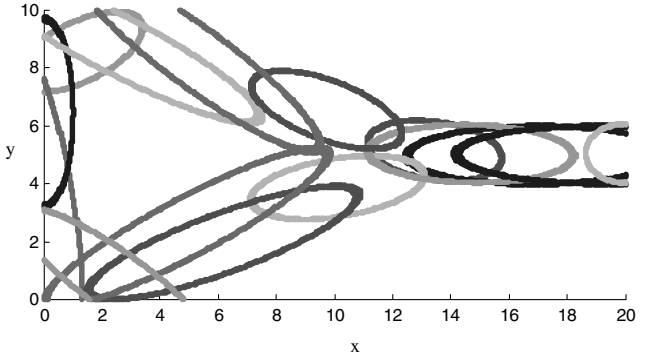

Fig. 14 Optimized locations and shapes of HRBFN bases for example 2.

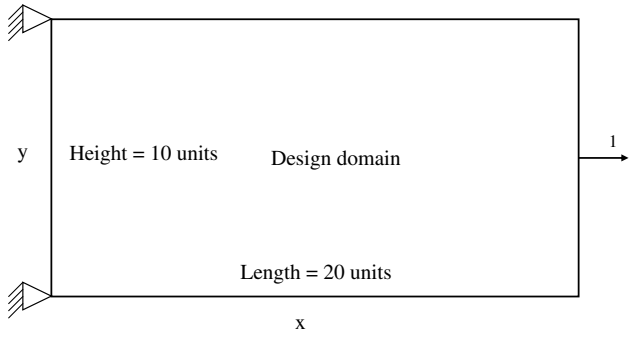

Fig. 12 Boundary conditions and loading for example 2, which uses a 20 × 10 FEA mesh.

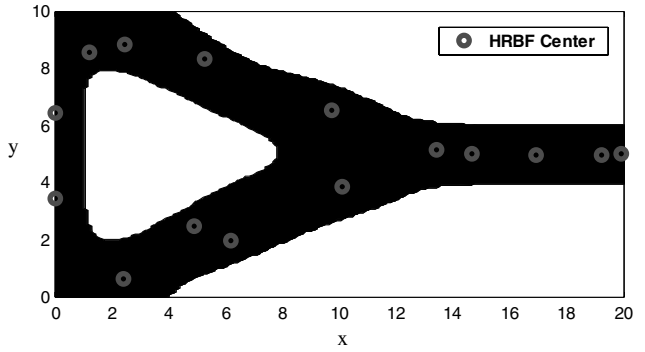

Fig. 15 Result of HRBFN-based topology optimization for example 2.

such that the network base can be located anywhere within the rectangular area under consideration. The angle parameter is such that it allows for any orientation of the network base. The width parameter is such that the network base can span the entire rectangular area under consideration. The lower and upper bounds on the HRBFN parameters for the example presented are as follows. For the weight parameter, $w_{\text{low}} = 0$ and $w_{\text{high}} = 1$ to ensure that the maximum density at the peak point for that base does not exceed 1. For the location parameter, $\bar{\mu}_{1\text{low}} = 0$, $\bar{\mu}_{1\text{high}} = 20$, $\bar{\mu}_{2\text{low}} = 0$, and $\bar{\mu}_{2\text{high}} = 10$, because a rectangular plate with a dimension of 20 units in the x direction and 10 units in the y direction is considered. For the width parameter, $\sigma_{1\text{low}} = 0.5$, $\sigma_{1\text{high}} = 4$, $\sigma_{2\text{low}} = 2$, and $\sigma_{2\text{high}} = 40$ to ensure that a network base is capable of spanning the entire breadth of the rectangular plate. For the angle parameter, $\theta_{\text{low}} = 0$ deg and $\theta_{\text{high}} = 180$ deg to ensure a network base can be oriented in any direction.

The next two examples presented use different mesh sizes, a different number of network bases, and complicated loading. Figure 12 (example 2) shows a cantilever beam fixed at the left edge and horizontal axial loading at the midpoint of the right edge. The objective is to get a minimum compliance design using 40% of the total material. Figure 13 shows the optimal topology obtained by the traditional method [12] using a 20×10 mesh. The same problem was solved using the proposed HRBFN TDF approach using 15 bases and the same mesh size. The number of bases to be selected is based on the anticipated topology. Note that each base (represented by six design variables) is capable of acting as a link in the final topology. Hence, the number of bases used in the design process must be greater than the maximum anticipated structural links in the final design. Although 15 bases are not required, they demonstrate the robustness of the proposed scheme. Some of these 15 bases are not active (low values for the weight variable) in the final design. Figure 14 shows the optimal locations and shapes of the bases obtained by the proposed approach. Figure 15 shows the filtered topology obtained by the proposed approach. The final topology obtained is based on a fixed number of elements and bases. In practical applications, a designer does not have the liberty to iteratively increase the number of finite elements to guarantee convergence to an exact topology. The size of the finite element

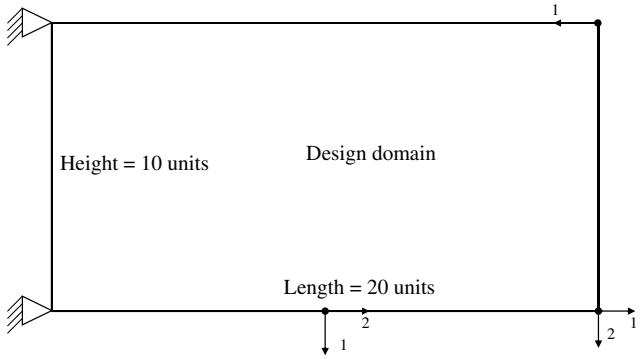

Fig. 16 Boundary conditions and loading for example 3, which uses a 20 × 10 FEA mesh.

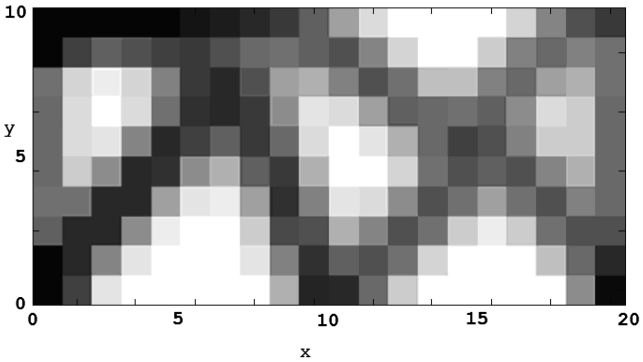

Fig. 17 Result of traditional SIMP topology optimization for example 3, unfiltered.

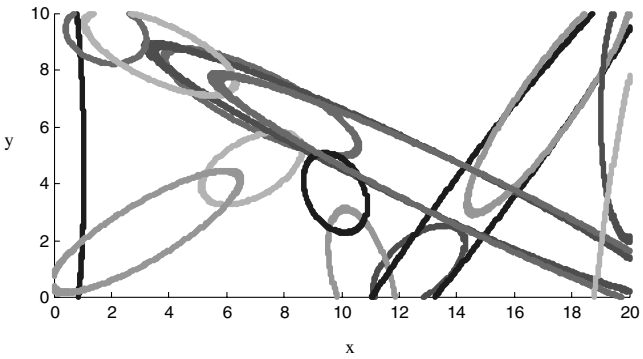

Fig. 18 Optimized locations and shapes of HRBFN bases for example 3.

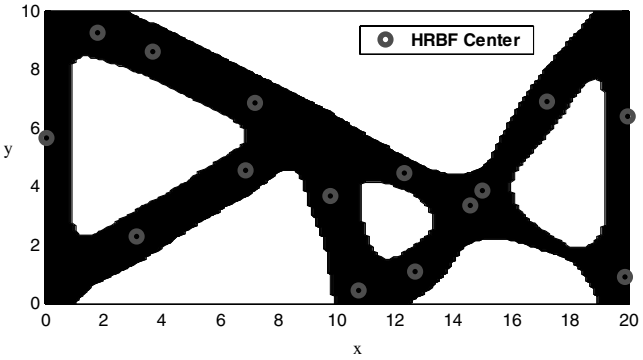

Fig. 19 Result of HRBFN-based topology optimization for example 3.

model is governed mostly by the memory and time constraints and the user's intuition. Hence, the results presented are for a fixed mesh size of 20×10.

Figure 16 shows a cantilever beam with complicated loading compared with the previous example. The objective is to get a minimum compliance design using 40% of the total material. Figure 17 shows the optimal topology obtained by the traditional method using a 20×10 mesh. Figure 18 shows the optimal basis locations and shapes obtained by the proposed approach with 15 bases and the same mesh size. Figure 19 shows the filtered topology obtained by the proposed approach.

VI. Conclusions

The application of the HRBFN as a TDF for topology optimization was demonstrated. A robust optimization algorithm was developed using perturbation and SLP. The algorithm was applied to solve minimum compliance topology optimization problems with encouraging results. The topologies obtained were free of checkerboard patterns and close to being manufacturable, thus demonstrating the potential of the proposed approach. An interactive software tool that allows users to graphically change the HRBFN parameters and, hence, the topology would further help satisfy exact manufacturability criteria. The compliance (objective) values of the topology manufactured would be quite close to the one obtained from theoretical topology design. This would be useful in designing topologies for sophisticated applications (e.g., compliant mechanisms) for which the objective function values (e.g., the output displacement of compliant mechanism) are critical. The application of the HRBFN as a TDF for maximum natural frequency design and the design of compliant mechanisms is under investigation. The application of the HRBFN to postprocessing results from commercial FEA software is under investigation, and we plan to present the results in a future paper.

References

[1] Bendsøe, M. P., and Kikuchi, N., "Generating Optimal Topologies in Optimal Design Using a Homogenization Method," *Computer Methods in Applied Mechanics and Engineering*, Vol. 71, No. 2, 1988, pp. 197–224.
doi:10.1016/0045-7825(88)90086-2

[2] Osher, S., and Sethian, J. A., "Fronts Propagating with Curvature-Dependent Speed: Algorithms Based on Hamilton–Jacobi Formulations," *Journal of Computational Physics*, Vol. 79, No. 1, 1988, pp. 12–49.
doi:10.1016/0021-9991(88)90002-2

[3] Stolpe, M., and Svanberg, K., "An Alternative Interpolation Scheme for Minimum Compliance Topology Optimization," *Structural and Multidisciplinary Optimization*, Vol. 22, No. 2, 2001, pp. 116–124.
doi:10.1007/s001580100129

[4] de Ruiter, M. J., and van Keulen, F., "Topology Optimization: Approaching the Material Distribution Problem Using a Topological Function Description," *Structural and Multidisciplinary Optimization*, Vol. 26, No. 6, 2004, pp. 406–416.
doi:10.1007/s00158-003-0375-7

[5] Bendsøe, M. P., "Optimal Shape Design as a Material Distribution Problem," *Structural and Multidisciplinary Optimization*, Vol. 1, No. 4, 1989, pp. 193–202.

[6] Wang, S. Y., Lim, K. M., Khoo, B. C., and Wang, M. Y., "An Extended Level Set Method for Shape and Topology Optimization," *Journal of Computational Physics*, Vol. 221, No. 1, 2007, pp. 395–421.
doi:10.1016/j.jcp.2006.06.029

[7] Poulsen, T. A., "Topology Optimization in Wavelet Space," *International Journal for Numerical Methods in Engineering*, Vol. 53, No. 3, 2002, pp. 567–582.
doi:10.1002/nme.285

[8] Cui, G. Y., Tai, K., and Wang, B. P., "Topology Optimization for Maximum Natural Frequency Using Simulated Annealing and Morphological Representation," *AIAA Journal*, Vol. 40, No. 3, 2002, pp. 586–589.

[9] Poggio, T., and Girosi, F., "A Theory of Networks for Approximation and Learning," Massachusetts Institute of Technology, Rept. 1140, July 1989; also Center for Biological Information Processing Paper 31.

[10] Poggio, Tomaso, and Girosi, Federico, "Network for Approximation and Learning," *Proceedings of the IEEE*, Vol. 78, No. 9, 1990, pp. 1481–1496.
doi:10.1109/5.58326

[11] Lyness, J. N., and Moler, C. B., "Numerical Differentiation of Analytical Functions," *SIAM Journal on Numerical Analysis*, Vol. 4, No. 2, 1967, pp. 202–210.
doi:10.1137/0704019

[12] Sigmund, O., "A 99 Line Topology Optimization Code Written in Matlab," *Structural and Multidisciplinary Optimization*, Vol. 21, No. 2, 2001, pp. 120–127.
doi:10.1007/s001580050176

N. Alexandrov
Associate Editor